The Astrophysical Journal Letters, 933:L31 (10pp), 2022 July 10 https://doi.org/10.3847/2041-8213/ac7950

Searching for a Hypervelocity White Dwarf SN Ia Companion: A Proper-motion Survey of SN 1006

Joshua V. Shields[1], Wolfgang Kerzendorf[1,2], Matthew W. Hosek, Jr.[3], Ken J. Shen[4], Armin Rest[5,6], Tuan Do[3], Jessica R. Lu[7], Andrew G. Fullard[1], Giovanni Strampelli[5], and Alfredo Zenteno[8]
[1] Department of Physics and Astronomy, Michigan State University, East Lansing, MI 48824, USA; shield90@msu.edu
[2] Department of Computational Mathematics, Science, and Engineering, Michigan State University, East Lansing, MI 48824, USA
[3] Department of Physics and Astronomy, University of California, Los Angeles, CA 90095, USA
[4] Department of Astronomy and Theoretical Astrophysics Center, University of California, Berkeley, CA 94720, USA
[5] Space Telescope Science Institute, 3700 San Martin Drive, Baltimore, MD 21218, USA
[6] Department of Physics and Astronomy, The Johns Hopkins University, 3400 North Charles Street, Baltimore, MD 21218, USA
[7] University of California, Berkeley, Department of Astronomy, Berkeley, CA 94720, USA
[8] Cerro Tololo Inter-American Observatory, NSFs National Optical-Infrared Astronomy Research Laboratory, Casilla 603, La Serena, Chile
Received 2022 May 17; revised 2022 June 10; accepted 2022 June 15; published 2022 July 8

Abstract

Type Ia supernovae (SNe Ia) are securely understood to come from the thermonuclear explosion of a white dwarf as a result of binary interaction, but the nature of that binary interaction and the secondary object is uncertain. Recently, a double white dwarf model known as the dynamically driven double-degenerate double-detonation (D6) model has become a promising explanation for these events. One realization of this scenario predicts that the companion may survive the explosion and reside within the remnant as a fast moving ($V_{\rm peculiar} > 1000$ km s^{-1}), overluminous ($L > 0.1\,L_{\odot}$) white dwarf. Recently, three objects that appear to have these unusual properties have been discovered in the Gaia survey. We obtained photometric observations of the SN Ia remnant SN 1006 with the Dark Energy Camera over four years to attempt to discover a similar star. We present a deep, high-precision astrometric proper-motion survey of the interior stellar population of the remnant. We rule out the existence of a high-proper-motion object consistent with our tested realization of the D6 scenario ($V_{\rm transverse} > 600$ km s^{-1} with $m_r < 21$ corresponding to an intrinsic luminosity of $L > 0.0176\,L_{\odot}$). We conclude that such a star does not exist within the remnant or is hidden from detection by either strong localized dust or the unlikely possibility of ejection from the binary system almost parallel to the line of sight.

Unified Astronomy Thesaurus concepts: Type Ia supernovae (1728); White dwarf stars (1799); Supernovae (1668); Supernova remnants (1667); Astrometry (80)

1. Introduction

Type Ia supernovae (SNe Ia) are well-studied, highly energetic events that are fundamental drivers of galactic chemical enrichment (Timmes et al. 1995; Nomoto et al. 2013; Kobayashi et al. 2020) and that led to the discovery of the accelerating expansion of the universe by allowing for secure measurements to distant galaxies (Riess et al. 1998; Perlmutter et al. 1999). Despite the central role that these energetic events play in our understanding of the universe and decades of focused research (e.g., see Maoz et al. 2014; Ruiz-Lapuente 2019), we still do not know the progenitor system and explosion scenario that create these events. SNe Ia arise from a carbon/oxygen white dwarf undergoing thermonuclear runaway (Pankey 1962; Colgate & McKee 1969), but the circumstances that lead to this condition are uncertain. A misunderstanding of the underlying physics will result in uncertainties in our understanding of the universe that is built upon these events.

SN Ia progenitor scenarios are divided into two broad classes. In one major scenario, a white dwarf violently merges with a secondary white dwarf, which leads to explosion (Iben & Tutukov 1984; Webbink 1984). In the other, the primary white dwarf accretes material from a nearby secondary, which also prompts thermonuclear runaway. This accretion scenario has many variations, with the secondary being either degenerate (Dan et al. 2011) or nondegenerate (Whelan & Iben 1973; Nomoto 1982; Iben et al. 1987; Livio 2000). Significant work has been done in attempting to disentangle progenitor scenarios and discover which, if any, of these processes are progenitors of SNe Ia, but finding strong support for any specific scenario has proven difficult (see Ruiz-Lapuente 2019 for a detailed discussion). One crucial, directly testable prediction comes from the secondary star in the binary system. In the violent merger scenario, the secondary is expected to be completely disrupted, while many accretion scenarios make the strong prediction that the secondary survives the explosion and exists within the resulting SN Ia remnant.

Identification of a surviving companion would lend powerful support to a corresponding accretion scenario based on the properties of the companion star (Marietta et al. 2000; Pakmor et al. 2008; Pan et al. 2012; Shappee et al. 2013a; Pan et al. 2013). Galactic SN Ia remnants have been the subject of much scrutiny to discover a surviving companion, but no such companion has been unambiguously identified (e.g., see Ruiz-Lapuente et al. 2004; Ihara et al. 2007; Hernández et al. 2009; Kerzendorf et al. 2009; Schaefer & Pagnotta 2012; Kerzendorf et al. 2014, 2018; Ruiz-Lapuente et al. 2018, 2019). These works focused on identifying bright, nondegenerate companions tying back to the nondegenerate accretion scenario.

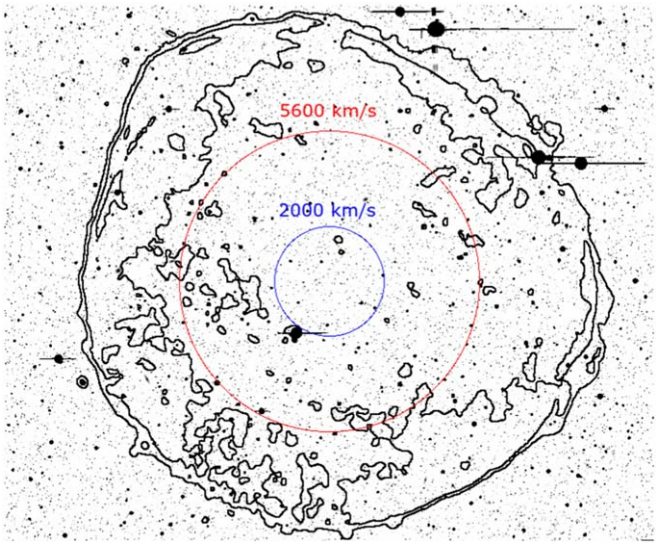

Figure 1. 2017 DECam imagery of the SN 1006 remnant. The contours are CHANDRA X-ray data (0.5–0.9 keV) showing the position of the remnant. The circles indicate the search region (red) and the likely maximum displacement of a D6 star (blue), as well as the physical transverse velocity of a star corresponding to the angular distance assuming a distance to the remnant. The larger search region allows for ambiguity in the center of the remnant.

However, mounting evidence including, but not limited to, nondetection of signatures of a nondegenerate companion in early (Hayden et al. 2010; Bianco et al. 2011; Bloom et al. 2012; Zheng et al. 2013; Olling et al. 2015; Marion et al. 2016; Shappee et al. 2016; Cartier et al. 2017; Miller et al. 2018; Shappee et al. 2018; Holmbo et al. 2019; Fausnaugh et al. 2021) as well as late times (Mattila et al. 2005; Leonard 2007; Shappee et al. 2013b; Lundqvist et al. 2013, 2015; Maguire et al. 2016; Sand et al. 2016; Graham et al. 2017; Woods et al. 2017; Sand et al. 2018; Vallely et al. 2019; Tucker et al. 2020) disfavor the nondegenerate accretion scenario as an explanation for the bulk of SNe Ia, aligning with the nondetection of a nondegenerate surviving companion. Coincidentally, most surviving companion searches did not go deep enough to discover faint degenerate companions (e.g., white dwarfs), which have recently come to the forefront of the SN Ia progenitor debate.

In this work, we test a specific realization of the Dynamically Driven Double-Degenerate Double-Detonation (D6) scenario (Guillochon et al. 2010; Pakmor et al. 2010, 2013; Shen & Bildsten 2014). In this scenario, the primary CO white dwarf undergoes unstable He accretion from a secondary degenerate He or CO white dwarf companion. The primary forms a thin He shell that detonates, which compresses the star and triggers thermonuclear runaway. If the He shell detonates early on in the accretion process, the secondary will survive the explosion and be flung out of the system with a minimum velocity of $1000\,\mathrm{km\,s^{-1}}$ (Shen et al. 2018), significantly above that inherited by normal processes of stellar evolution, barring specific dynamic interactions in the galactic center, which are exceedingly rare (Hills 1988; Brown 2015; Generozov & Perets 2022). Shen et al. (2018) discovered three hypervelocity white dwarfs in the field in the Gaia mission (Collaboration et al. 2016, 2018a) that lie in a peculiar region of the color luminosity diagram, aligning with this realization and providing the most powerful observational support that any progenitor scenario has seen. Combined with the mounting evidence against other established SNe Ia progenitor scenarios, this discovery suggests the possibility that most if not all normal SNe Ia arise from the D6 scenario.

This scenario provides a testable hypothesis. If this realization of the D6 scenario is the generic explanation for SNe Ia, each SN Ia remnant must contain such a surviving companion. The SN ejecta that forms the remnant is ejected with a mean velocity $V_{\mathrm{ejecta,\ mean}} \simeq 5000\,\mathrm{km\,s^{-1}}$ and a maximum velocity $V_{\mathrm{ejecta,max}} \geqslant 20000\,\mathrm{km\,s^{-1}}$ (see, e.g., Hillebrandt & Niemeyer 2000), far above the surviving companion's velocity. The ejecta slows upon colliding with the surrounding interstellar medium but still leaves the companion contained by the SN remnant. We intended to test this realization of the D6 scenario by searching for a surviving D6 companion inside the SN 1006 remnant, which is uniquely suited to such a search. Galactic SN remnants generally trace the stellar population and therefore reside primarily within the Galactic plane (mean and standard deviation of the Galactic remnant latitudes $b = 0.117 \pm 2.^{\circ}787$; Green 2019), which creates two significant problems: First, the Galactic plane is heavily obscured by dust and is prohibitively difficult to search for faint, blue objects (e.g., white dwarfs, see Ruiz-Lapuente et al. 2018) with current observational constraints. Second, there is a high density of contaminating foreground and background interlopers, which has two effects. The high density can contribute to source confusion and force the search to include sources that cannot be placed in front of or behind the remnant, obfuscating the search to the point of infeasibility. SN 1006 uniquely resides nearby and high above the galactic plane with a galactic latitude $b = 14.^{\circ}6$ and a distance $d = 2.17 \pm 0.08$ kpc (Winkler et al. 2002),[9] leading to shallow foreground extinction ($A_v = 0.2154 \pm 0.0564$) and relatively little source confusion. Furthermore, a star moving $1000\,\mathrm{km\,s^{-1}}$ in a transverse direction at such a close distance would show a very strong proper-motion signal of 97.2 mas $\mathrm{yr^{-1}}$, far above the normal positional uncertainties of high-precision astrometric measurements. These properties indicate that a high-velocity D6 companion will be observable within the remnant if one exists.

There have been multiple previous searches in SN 1006 for surviving companions, but they largely focused on discovering bright, nondegenerate donors and did not go deep or wide enough to discover a compact high-velocity object in line with the predictions of the D6 scenario (e.g., Hernandez et al. 2012 down to $m_r = 15$; Kerzendorf et al. 2012 down to $m_v = 19$ but with a search radius of $r = 2'$). Furthermore, a D6 star in SN 1006 would have only had about 10^3 yr to evolve, orders of magnitude less time than the three candidates discovered in the field in Shen et al. (2018), which are thought to be at least 10^5 yr postexplosion. Liu et al. (2021) showed that a D6 star will be significantly overluminous within 10^4 yr, but the appearance of a D6 star as young as that in SN 1006 has not yet been observed, and an unusually high velocity remains the strongest signature of such an object. While Kerzendorf et al. (2017) went down to $m_r = 21$ and directly sought to investigate the possibility of a white dwarf companion, a young D6 star's heavily uncertain appearance in color and luminosity could

[9] We note that there is some ambiguity on the distance to the remnant. Kerzendorf et al. (2017) report the distance to be 2.07 kpc ± 0.18, but Winkler et al. (2002) report 2.17 ± 0.08. We adopt this distance for the remainder of this work.

mean that it resides far off the standard white dwarf cooling track, which might have caused the star to elude this analysis as well.

In this work, we present a deep 4 yr baseline astrometric proper-motion survey of the stars inside SN 1006 using the Dark Energy Camera (Diehl 2012; Flaugher et al. 2015) to find the surviving companion predicted by the Shen et al. (2018) realization of the D6 hypothesis. We measured and report the proper motions of over 2000 objects beyond the detection limit of Gaia.

In Section 2, we present our observations and initial data reduction. In Section 3, we detail our astrometry and proper-motion extraction. In Section 4, we present the results of our survey and the constraints on a surviving companion in SN 1006 that follow. In Section 5, we consider confounding possibilities of nondetection and discuss the high-proper-motion objects identified in our search. We conclude by summarizing our findings and discussing future work in Section 6.

2. Observations and Data Reduction

For our work, we acquired preexisting photometry of the SN 1006 remnant from the nights of 2017 January 30 and 2018 May 22, and obtained new observations of the remnant on the night of 2021 January 22, shown in Figure 1. All data were captured using the Dark Energy Camera (Diehl 2012; Flaugher et al. 2015) instrument mounted on the 4-m Blanco telescope located at the Cerro Tololo Inter-American Observatory (CTIO). Exposures were taken in five bands, but all data processing and analysis were performed on *r*-band observations to minimize atmospheric scattering as well as foreground dust extinction, allowing for higher astrometric accuracy and better measurements of faint, reddened sources. All *r*-band exposures were 50 s, stacked to create combined exposure times of 250 or 300 s depending on the epoch.

After standard calibration (bias correction, flat-fielding, and WCS) was done by the NSF NOIRLab DECam Community Pipeline (Valdes et al. 2014), we reduced the data using the `Photpipe` pipeline as described in Rest et al. (2005, 2013): Images were warped into a tangent plane of the sky using the "SWarp" routine (Bertin et al. 2002) before photometry of the stellar sources is obtained using the standard point-spread function (PSF) fitting software DoPHOT (Schechter et al. 1993). We obtained observations of standard stars on the same nights as the photometric catalogs, which we used for calibration to obtain our photometric zero-points.

Each epoch comprised either five or six dithered observations, which were combined for each of the 62 individual CCDs. Multiple observations of the same star within one pixel coordinate ($0\farcs263$) were matched and combined. Additional details about this initial matching are given in Appendix B. Final stellar positions were then calculated using uncertainty-weighted averages in both CCD pixel dimensions, and their uncertainties coadded using standard uncertainty propagation rules, decreasing uncertainties by a factor of $1/\sqrt{N}$. We note that, as dithering patterns did not observe all sources in each image, this factor was inconsistent depending on source position inside a CCD. With secure single epoch catalog positions, we then needed to cross-match sources across epochs to identify their movement and extract proper motions.

3. Methodology and Analysis

A source moving inside SN 1006 at $1000\,\mathrm{km\,s^{-1}}$, the minimum velocity in line with the predictions of the D6 scenario (Shen et al. 2018), would have a proper motion of $97\,\mathrm{mas\,yr^{-1}}$ assuming our chosen distance to the remnant of 2.17 kpc. We initially set out to discover any star within SN 1006 with a proper motion higher than $80\,\mathrm{mas\,yr^{-1}}$ with no further restrictions other than being bright enough to be measurable in the DECam imagery. To recover proper motions with sufficient signal to noise to identify a surviving companion, we needed to discover a transformation from each individual instrumental CCD reference frame into one common reference frame. We chose to use the Gaia EDR3 catalog (Gaia Collaboration et al. 2021) to establish this common astrometric reference frame because it is currently the publicly available catalog with the most precisely measured positions of the stars inside the remnant.

3.1. Building Our Proper-motion Catalog

We began by identifying a grid of 16 bright stars on each CCD with relatively small astrometric position uncertainties (see Equation (A1) in Appendix A) that could be matched between our DECam and Gaia source catalogs. We used these as an initial guess for a second-degree polynomial (12 free parameters) that transforms from our DECam pixel coordinates to Gaia ICRS coordinates. Using this initial guess, we matched additional sources within $1''$ (3.8 pixels) and 1 mag in the DECam and Gaia catalogs and refit the polynomial transformation. We note that Gaia *G* band and DECam *r* band are different filters, but we found that empirically the two bands are similar (the *r*-band magnitude and *G*-band magnitude have a mean difference of 0.02 mag in our sample). The filters are also centered on similar wavelengths. Additionally, the magnitude matching was only used as a conservative safeguard against spurious matches. We finally performed a second iteration of this fitting process, matching the DECam catalog to the Gaia catalog with a polynomial of up to fourth degree (30 free parameters) beginning with the previously matched stars as our initial guess to capture minor instrumental distortions. Between 4000 and 9000 stars were identified and matched between the Gaia and DECam catalogs in each CCD for this polynomial fitting step. Both iterations of the polynomial transformation were tested over a small range of polynomial orders to arrive at a transformation that produced strong agreement between Gaia and DECam positions.

With this final polynomial transformation from the DECam instrumental reference frame to the Gaia ICRS defined reference frame, we matched DECam objects across all three epochs within $1''$ and fit their motions independently in R.A. and decl. using χ^2 minimization. Only stars detected in all three epochs were fit for proper motion. Final proper-motion uncertainties are shown in Figure 2. Uncertainties here are calculated using standard uncertainty propagation rules from χ^2 minimization. The structure in the multiple systematic uncertainty floors seen in the figure traces back to stars at the edges of fields being observed in incomplete fractions of the imaging dithering patterns. For all but the faintest objects, our proper motions have uncertainties at least three times smaller than our desired signal of $80\,\mathrm{mas\,yr^{-1}}$. We show additional independent verification of our proper-motion measurements and comparisons to Gaia in Appendix C. Relative to Gaia, we

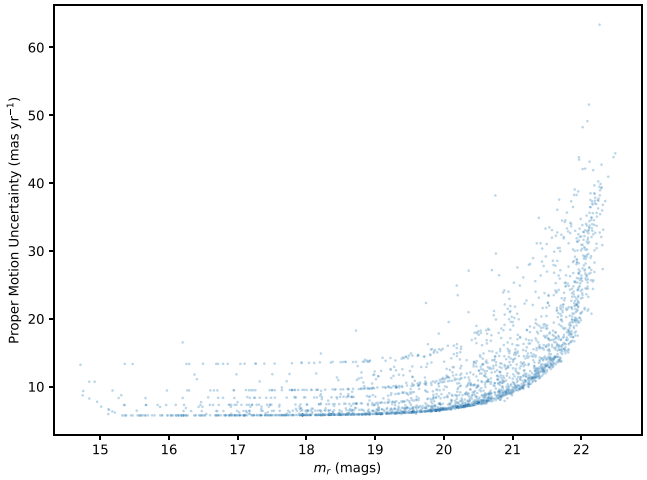

Figure 2. Proper-motion uncertainty vs. r-band magnitude. There are different systematic uncertainty floors depending on CCD dithering and number of observations for a source. The desired signal measurement was 80 mas yr^{-1}.

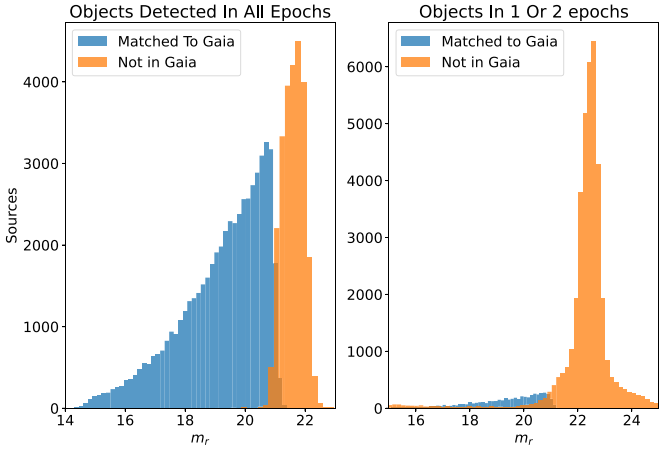

Figure 3. Histograms of all sources discovered in our search divided into sources observed in all three epochs or in an incomplete fraction. We only extracted proper motions for objects discovered in all three epochs.

find that over our whole sample, our proper-motion measurements have an rms difference average of 5.61 mas yr^{-1} and rms standard deviation of 5.14 mas yr^{-1}. This observed scatter is also much smaller than our desired signal of 80 mas yr^{-1}, allowing for proper-motion measurements of sufficient quality to detect a surviving D6 companion within the remnant.

3.2. Search Region and Parameter Restrictions

The site of the SN Ia event that created SN 1006 is uncertain because density variations in the interstellar medium might have led to a significant offset between the geometric center of the remnant and the site of the explosion (Winkler et al. 2005; Williams et al. 2013). We restricted our search to a 9′ cone corresponding to a transverse velocity of ∼5600 km s^{-1} at a distance of 2.17 kpc, centered on the geometric center of SN 1006 reported as $15^{h}02^{m}55\overset{s}{.}4$, −41°56′33″ by Winkler et al. 2002, shown in Figure 1. This transverse velocity is far higher than the upper limit on the velocity expected for a surviving companion (Shen & Schwab 2017), but the cone radius was chosen to allow for strong ambiguity on the site of the explosion. Furthermore, because of this ambiguity, we made no directional proper-motion cuts. This left us with 8123 stars for analysis. Our final catalog can be found at https://doi.org/10.5281/zenodo.6506198, which includes 125,116 sources both in and around the remnant, with sources delineated as either inside or outside the search region.

4. Results

We conducted a high-precision proper-motion astrometric survey of the stars within SN 1006 to search for a surviving companion predicted by the D6 scenario. In our sample, Gaia completeness appears to drop rapidly at $m_r = 21$ (see Figure 3). Inside the remnant, Gaia contains 5341 stars. We augmented the survey by measuring the proper motions of 2782 stars up to three magnitudes fainter than Gaia was able to detect. We comment on the high-proper-motion objects discovered at these faint magnitudes in Section 5, but we chose $m_r = 21$ as the limiting magnitude for this work for three reasons: First, beyond this magnitude limit there are no available color or parallax measurements for our objects, which makes it difficult to verify an object's identity as a surviving D6 companion. Second, completeness begins dropping quickly, which can be seen by the large number of objects detected in an incomplete fraction of our observations in Figure 3. Third, proper-motion uncertainties systematically grow beyond a third of our desired signal of 80 mas yr^{-1} (see Figure A1 in Appendix A and Figure 4).

Our limiting magnitude is multiple magnitudes fainter than a D6 star is expected to appear within the SN 1006 remnant. A D6 star similar to those discovered by Shen et al. (2018) would appear between $17.5 < m_r < 19.2$. However, the three D6 candidates discovered in that work reside within the field, having likely had over 10^5 yr to radiate away excess energy injected from the explosion of the primary and reestablish equilibrium appearances. Liu et al. (2021) simulated the appearance of a D6 star shortly after explosion and found that the star would possess a luminosity of 10 $L_\odot$ ($m_r \approx 14.2$ in SN 1006) 10^3 yr after the explosion and remain above 1 $L_\odot$ ($m_r \approx 16.7$ in SN 1006) for 10^7 yr. However, a D6 candidate as young as what would appear in SN 1006 (10^3 yr post-SN) has not yet been observed. Thus, for our search, we conservatively considered all stars down to a magnitude of $m_r = 21$. Additionally, while a D6 star inside the remnant is expected to possess a velocity of >1000 km s^{-1}, we initially considered down to a projected velocity equivalent of 800 km s^{-1} to allow for a hidden radial-velocity component and to compensate for measurement error. We then expanded our proper-motion cut, detailed in the following paragraph.

The results of our Gaia-DECam survey are shown in Figure 4. We show the three previous D6 candidates from Shen et al. (2018), the expected parameter space of a similar star inside SN 1006, as well as our conservative limiting magnitude and proper-motion cuts. We did not discover any high-proper-motion object in this space brighter than $m_r = 21$. To investigate the possibility of a high-proper-motion object slower than that expected a priori, we investigated the 22 fastest of the 8123 stars within the remnant (the percentile equivalent of the 3σ highest-proper-motion outliers). Of these, 18 are too faint to be supported as the surviving companion ($m_r > 21$) without the additional follow-up needed to rule each out from being a contaminating foreground star, a contaminating halo star, or from having a nonphysical proper-motion measurement due to an undersampled (PSF), which leads to poor localization. The remaining four candidates are reported in Table 1 under their Gaia identifiers and are marked in Figure 4,

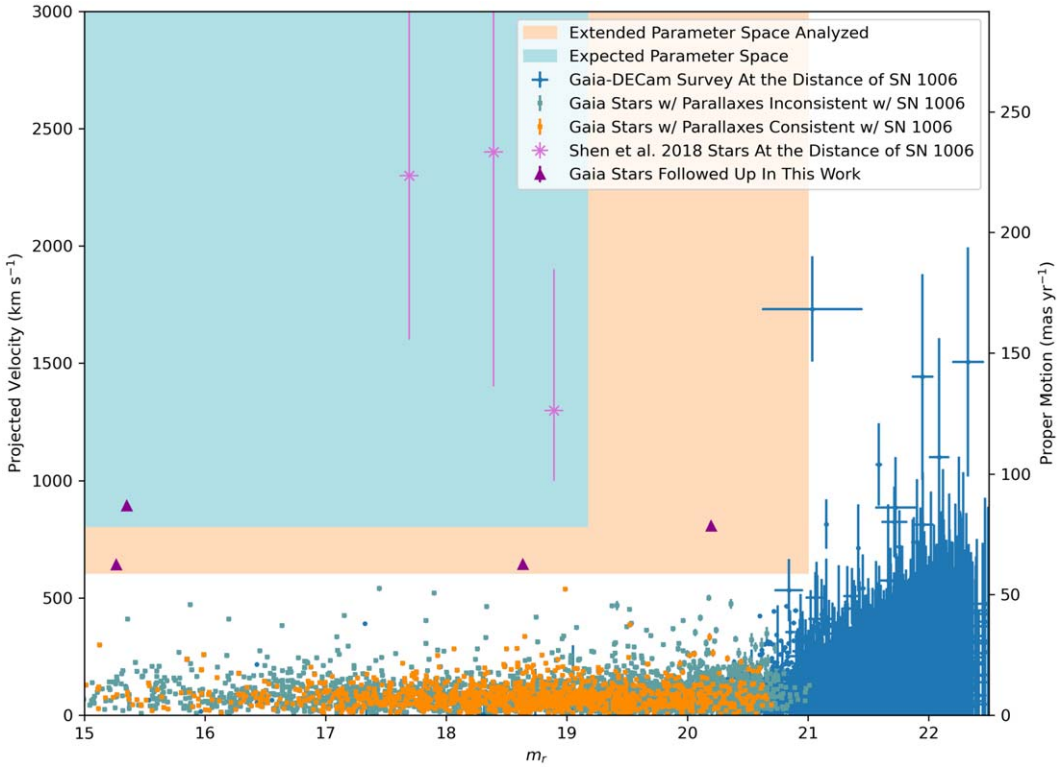

Figure 4. Results of the proper-motion survey showing the apparent *r*-band magnitude against proper-motion measurement and calculated transverse velocities assuming a distance of 2.17 kpc for DECam sources. The three Shen et al. (2018) stars have corrected apparent magnitudes as they would appear at the same distance with uncertainties and including foreground extinction. A surviving white dwarf companion in accordance with the predictions of the D6 scenario was expected to lie in the shaded region with the previously discovered D6 stars. The four Gaia stars in the analyzed region are shown in Table 1 and Figure 5 and are discussed in Section 4 along with the high-proper-motion objects fainter than 21.

Table 1
High-proper-motion Gaia Sources in SN 1006

Gaia Source ID	m_G	$G_{BP} - G_{RP}$	m_r	Parallax (mas)	Proper Motion (mas yr^{-1})	Projected Velocity Inside Rem (km s^{-1})
6004785431417429120	15.35	1.87	15.35	3.37 ± 0.04	67.4 ± 0.1	693.3 ± 1.0
6004784984740826752	20.20	2.60	20.20	2.16 ± 0.81	82.2 ± 1.4	845.6 ± 14.4
6004735811668137472	18.64	1.51	18.64	0.62 ± 0.27	44.2 ± 0.4	454.7 ± 4.1
6004735094407417344	15.26	1.81	15.26	3.48 ± 0.04	60.2 ± 0.1	619.3 ± 1.0

Note. Projected velocity assumes a distance of 2.17 kpc and not a distance implied by the parallax measurement in case of a spurious parallax measurement that would cause us to miss a surviving companion. Proper motions shown here are Gaia-reported measurements.

reaching down to a proper motion of 62.5 mas yr^{-1} or a projected velocity of 616 km s^{-1}. We additionally show a color–magnitude diagram of these four stars, the three D6 candidates from Shen et al. (2018), as well as a sample of 150,000 Gaia stars with secure parallax measurements (parallax_over_error >30) in and around the remnant in Figure 5. Unlike the three D6 candidates, the high-proper-motion Gaia stars in SN 1006 exist firmly on the main sequence and are each therefore unlikely to be the surviving companion. Additionally, Gaia EDR3 6004735811668137472 is the only object possessing a parallax that places it inside the remnant within uncertainties, while the other three have parallax measurements that point to foreground star identifications.

4.1. Constraints on Intrinsic Stellar Luminosity

We investigated the intrinsic luminosity constraints of our survey. To estimate the foreground extinction between us and the SN 1006 remnant, we used the Guo et al. (2021) southern sky three-dimensional dust maps, shown in Figure 6. The map queried at the distance of the remnant gives an extinction $E_{B-V} = 0.0673 \pm 0.0176$. Assuming an $R_V = 3.1$ F99 reddening law following Schlafly & Finkbeiner (2011), we calculate $A_V = 0.2154 \pm 0.0564$. Furthermore, using a resulting $A_r/A_V = 0.89$, we estimate $A_r = 0.192 \pm 0.050$. Adopting $A_r = 0.192$, a distance modulus of 11.68 corresponding to a distance of 2.17 kpc, and a bolometric magnitude equal to *r* band, an $m_r = 21$ object possesses an intrinsic luminosity of $L = 0.0176\, L_\odot$. We did not detect a high-proper-motion object with unusual colors brighter than this luminosity within SN 1006.

5. Discussion

We have investigated a prediction of one realization of the D6 scenario which might be a generic explanation for SNe Ia.

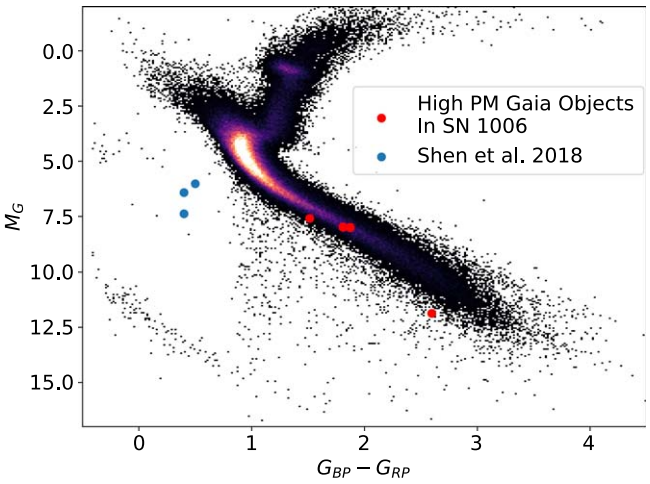

Figure 5. Color–magnitude Diagram of 150,000 secure-parallax (parallax over error >30) Gaia stars around SN 1006. The blue dots show the three D6 candidates discovered in the field by Shen et al. (2018) far off the main sequence. The red dots show the high-proper-motion (>500 km s^{-1}) Gaia objects inside SN 1006 in our search. They lie on or close to the main sequence with ordinary colors.

We have no observationally motivated constraints for how a D6 star would appear shortly after the explosion of the primary. The three candidates presented in Shen et al. (2018) were discovered in the field of the galaxy and are estimated to be older than $\sim 10^5$ yr postexplosion. Theory suggests that a young D6 star would be brighter than $m_r > 19$, but a significant inherited velocity remains the strongest observable property of such a star. We have investigated the stars in SN 1006 for this signature. Our survey places strict limits on the parameter space that a surviving D6 companion could exist inside SN 1006. Previous direct searches went down to $m_r = 15$ (Hernandez et al. 2012) and $m_V = 19$ (Kerzendorf et al. 2012). Kerzendorf et al. (2017) went down to $m_r = 21$ but only sought to investigate objects closely following the white dwarf cooling track. Here, we rule out the possibility of a high-velocity surviving companion in the remnant down to $m_r = 21$.

5.1. Confounding Possibilities

We did not detect an overluminous surviving white dwarf companion with a high-enough proper motion to be consistent with the D6 scenario inside SN 1006. We explored possibilities for a surviving D6 companion to have gone undetected in our analysis. Our search targeted stars with large transverse velocities detectable through proper-motion measurements. As a result, we identified two following outstanding reasons that a D6 star in the remnant might have gone undetected in our study: First, the star may have inherited an exceedingly large radial velocity with a small transverse velocity by being ejected almost parallel to our line of sight. Second, the star may be hidden by significant, unforeseen dust obscuration prompted by interaction with the SN.

We explore the possibility that a star launched with a significant velocity in a random direction did not inherit a large transverse velocity, with the majority of the velocity hidden in the radial direction. We performed a Monte Carlo simulation of a star launched in a random direction with a velocity of 1000 km s^{-1}, the lowest theoretically predicted velocity of a D6 star. The resulting probability distribution of the observed tangential velocity measured for such a star is presented in Figure 7. Our experiment and analysis would have detected the star above 94.3% of the time. However, a D6 star likely inherits a velocity far greater than 1000 km s^{-1}, quickly shrinking the unexamined portion of this distribution (e.g., a 1200 km s^{-1} star would have been discovered 97.3% of the time). This parameter space could be examined with detailed radial-velocity measurements of the stars in SN 1006 but remains a small, outstanding possibility.

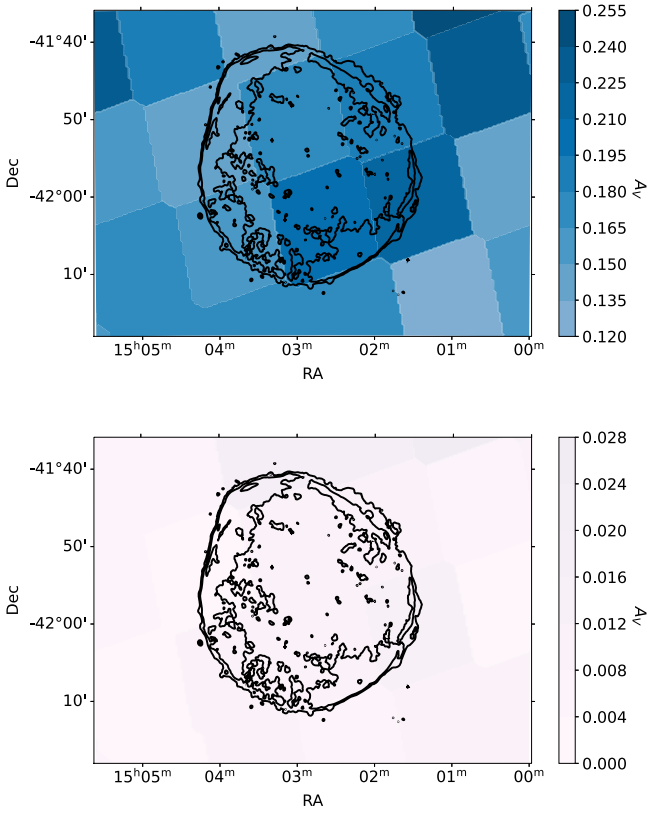

Figure 6. Guo et al. (2021) three-dimensional dust maps sampled in the direction of the SN 1006 remnant with X-ray contours displayed to show the position of the remnant. The top shows the maps sampled at the distance of the remnant (2.17 kpc). The bottom shows the difference between the absorption sampled at 1.94 and 2.41 kpc (2.17 ± 0.24, three standard deviations of the uncertainty on the distance, 0.08, respectively). Both maps are placed on a consistent color scale to emphasize the lack of additional dust extinction measured within the remnant. A_V is calculated assuming $E_{B-V} = 3.1A_V$ following Schlafly & Finkbeiner (2011).

We also consider the possibility that a D6 star could have been heavily enshrouded by dust from the remnant and thus appeared fainter than 21st magnitude in *r*-band. In Figure 6, we show the *V*-band absorption enclosed by the remnant, approximated by sampling the Guo et al. (2021) dust maps in front of and behind three times the uncertainty on the distance to the remnant. We see no evidence of additional dust absorption in the remnant on large-enough scales to be detectable by these dust maps, with an angular resolution of 13.′7. Any obscuring dust capable of hiding the surviving companion would need to be localized around the star itself, such as dust produced by a strong stellar wind prompted by interaction with the SN explosion.

5.2. Faint High-proper-motion Outliers

As a result of this survey, we discovered six faint, high-proper-motion objects between 21 and 22.5 mag listed in

Table 2
Discovered Faint High-proper-motion Objects in SN 1006

Target	R.A. (deg)	Decl. (deg)	m_r	Proper Motion (mas yr^{-1})	Projected Velocity (km s^{-1})
Candidate 1	225.618762	−41.856965	22.33	146.4 ± 47.3	1506.0 ± 486.6
Candidate 2	225.801826	−42.041687	22.09	107.0 ± 49.1	1100.7 ± 505.1
Candidate 3	225.823198	−42.064307	21.73	86.0 ± 21.0	884.7 ± 216.0
Candidate 4	225.697236	−41.985479	21.72	80.2 ± 14.6	825.0 ± 150.2
Candidate 5	225.916877	−41.995497	21.59	103.9 ± 17.1	1068.8 ± 175.9
Candidate 6	225.586830	−41.888318	21.04	168.3 ± 21.8	1731.0 ± 224.1

Notes. Projected velocity assumes a distance of 2.17 kpc. These objects are too faint to be supported as D6 candidates in this work but remain interesting candidates. Additionally, we investigated candidate 6 and found it to have an unreliable measurement due to its PSF overlapping with a nearby bright star.

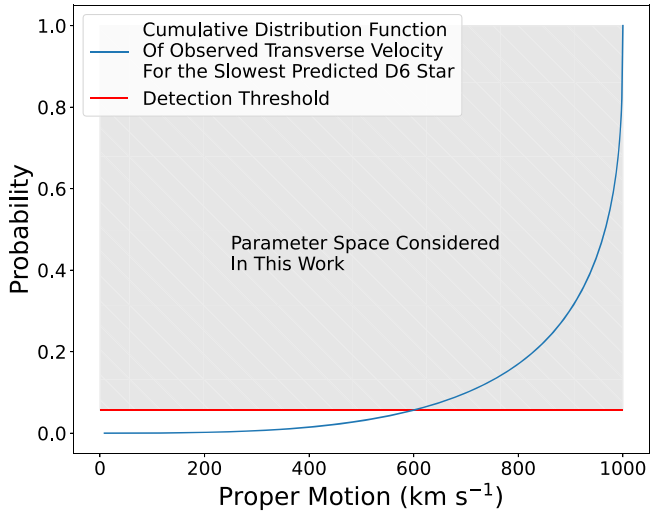

Figure 7. Results of our Monte Carlo simulation showing the observed transverse velocity of a 1000 km s^{-1} star, the minimum expected velocity of a D6 star, traveling in a random direction. We examined all stars with proper motions corresponding to transverse velocities of above 600 km s^{-1} or proper motions of 58.3 mas yr^{-1} (the top 22 proper-motion objects in our survey). As shown, this corresponds to examining 94.3% of this distribution. A faster velocity quickly shrinks the probability space, effectively moving farther down the shallow tail of the distribution.

Table 2 and seen in the faint end of Figure 4. These objects are too faint to have color information, and we note that these objects have large proper-motion uncertainties due to their poorly constrained initial positions tracing back to their faint appearances, and thus the objects are mostly less than 1σ or 2σ above our velocity threshold. While one of these objects may be the surviving companion in line with the significant dust obscuration scenario detailed above, we note that each is also likely a result of statistical sampling uncertainties and the large number of sources examined. Furthermore, we examined the Spitzer Enhanced Imaging Products (Fazio et al. 2004; Werner et al. 2004; Capak) combined 3.6, 4.5, 5.8, and 8.0 μm image catalog for coincident infrared sources with our high-proper-motion objects and did not discover any aligned sources. This provides strong evidence against dust obscuration, as absorbed light should be reradiated in the infrared and make the source easily detectable. We however note that spectral follow-up of these objects would concretely support or reject their respective statuses as the surviving companion by providing both color information that could place them on the main sequence or in an unusual portion of the color–magnitude diagram, as well as radial-velocity measurements that could support or oppose high intrinsic velocities as opposed to modest intrinsic velocities that appear large due to foreground nature.

6. Conclusions and Future Work

We present a deep 4 yr baseline astrometric survey of the stars in the SN 1006 remnant. We do not detect an overluminous, high-proper-motion white dwarf similar to that predicted by a realization of the D6 scenario presented in Shen et al. (2018). This result suggests that this realization of the D6 scenario is not generically responsible for SNe Ia. Alternatively, this result might be in line with the recent result of Pakmor et al. (2022), who showed that an SN Ia–like event can be created through the detonation of both the primary and the secondary white dwarf in the D6 scenario.

We investigated the possibility that a surviving companion star similar to or brighter than those detected in the field could have gone undetected in our study. We find that:

1. There is less than a 5.7% chance that a star with an intrinsic velocity of 1000 km s^{-1} could have been ejected from the system almost parallel to our line of sight, and have inherited a small-enough proper motion to have remained undetected. This possibility shrinks quickly as the velocity of the surviving companion increases.
2. There is no significant additional large-scale dust created by or coincident with the SN remnant. Dust capable of obscuring the surviving companion would need to be on angular scales significantly smaller than 13.′7 or a physical scale of 8.6 pc at the distance of the remnant, localized around the surviving companion itself.

We briefly consider the possibility of detecting a surviving D6 companion with an assumed luminosity of about 0.1 $L_\odot$ in other Galactic SN Ia remnants. We did not detect an unambiguous, overluminous white dwarf companion inside SN 1006 as predicted by our tested realization of the D6 theory; however, there exist tens of SN Ia remnants in the galaxy where a similar study could potentially be performed to search for a similar star. Upon inspection, we find that only three unambiguously classified SN Ia remnants exist with comparable distances to SN 1006, where a D6 star is approaching detection limits. These three remnants are RCW 86, Tycho's supernova remnant, and G272.2–3.2. These remnants all lie within or close to the Galactic plane behind 4.4, 3.5, and 2.6 magnitudes of V-band extinction, respectively (Schlafly & Finkbeiner 2011). This poses a challenging obstacle for repeating a high-precision proper-motion survey within these remnants, where a 0.1 $L_\odot$ star could be as faint as $m_r \sim 24$.

7. Contributor Roles

1. Conceptualization: Joshua V. Shields, Wolfgang Kerzendorf, Ken J. Shen.
2. Data curation: Joshua V. Shields, Armin Rest, Giovanni Strampelli.
3. Formal Analysis: Joshua V. Shields, Armin Rest.
4. Funding acquisition: Wolfgang Kerzendorf.
5. Investigation: Joshua V. Shields, Wolfgang Kerzendorf, Alfredo Zenteno.
6. Methodology: Joshua V. Shields, Matthew W. Hosek Jr., Armin Rest, Ken J. Shen, Tuan Do.
7. Project administration: Wolfgang Kerzendorf.
8. Resources: Armin Rest.
9. Software: Jessica R. Lu, Matthew W. Hosek Jr., Armin Rest.
10. Supervision: Wolfgang Kerzendorf.
11. Validation: Joshua V. Shields.
12. Visualization: Joshua V. Shields.
13. Writing—original draft: Joshua V. Shields, Wolfgang Kerzendorf.
14. Writing—review & editing: Joshua V. Shields, Wolfgang Kerzendorf, Matthew W. Hosek Jr., Ken J. Shen, Tuan Do, Andrew G. Fullard.

We thank the anonymous referee for helpful comments that improved the clarity and structure of this Letter.

AGF is supported by HST-AR-16613.002-A. Financial support for KJS was provided by NASA/ESA Hubble Space Telescope program #15871.

This work has made use of data from the European Space Agency (ESA) mission Gaia (https://www.cosmos.esa.int/gaia), processed by the Gaia Data Processing and Analysis Consortium (DPAC, https://www.cosmos.esa.int/web/gaia/dpac/consortium). Funding for the DPAC has been provided by national institutions, in particular the institutions participating in the Gaia Multilateral Agreement.

This work is based [in part] on observations made with the Spitzer Space Telescope, which is operated by the Jet Propulsion Laboratory, California Institute of Technology under a contract with NASA.

Facility: IRSA, Spitzer.

Software: Astropy (The Astropy Collaboration et al. 2013; Collaboration et al. 2018b), Scipy (Virtanen et al. 2020), Numpy (Harris et al. 2020), pandas (Reback 2022), Pyregions (Bradley et al. 2022), Matplotlib (Hunter 2007), DoPHOT (Schechter et al. 1993), SWarp (Bertin et al. 2002), DECam Community Pipeline (Valdes et al. 2014).

Appendix A
Position Uncertainty Estimation

We estimated the uncertainty of a single observation from the Dark Energy Camera following Rest et al. (2013):

$$\sigma_{\rm pix} = 0.1^2 + 1.5\left(\frac{\rm FWHM}{\rm S/N}\right)^2. \quad \text{(A1)}$$

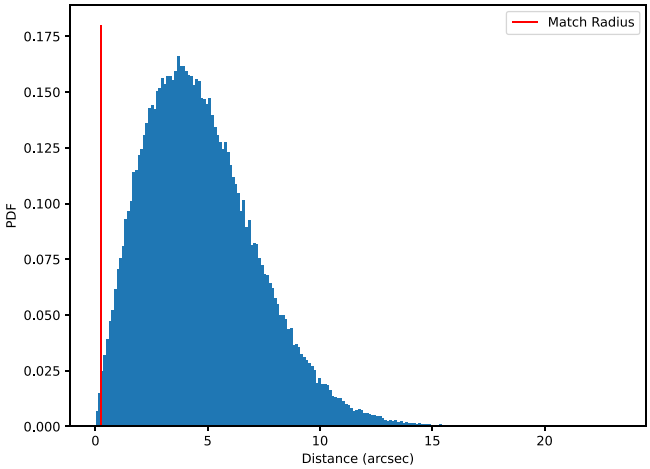

Figure 8. Nearest neighbor distribution function for a sample CCD after the initial stellar matching was completed. We adopted a search radius of 1 pixel or 0.″263 for our initial matching algorithm, a small-enough search radius to not allow for significant source confusion at the stellar density of the field.

Appendix B
Matching Algorithm Choices

To create our individual epoch catalogs, we combined detections of sources with two or more observations using the SCIPY.SPATIAL.KDTREE package to subdivide the parameter space and reduce the considered associations. We disregarded sources within 3 pixels from the edge of an observation, and only matched stars within 1 pixel or 0.″263. We chose this search radius, taking into consideration the stellar density of roughly one in eight pixels. Additionally, the nearest neighbor distribution function is shown in Figure 8, which shows that the nearest neighbor of a source is farther than 0.″263 away in almost all cases. A source could be matched with an unrelated object if it is both within the search region of the unrelated source and is not detected in a given epoch. This likely has the effect of artificially increasing proper motions, as the source would be reported as having moved anomalously far between epochs and is much more likely to be an issue for faint objects. This effect may explain some of the faint, high-proper-motion objects in our sample.

Appendix C
Proper Motion and Position Measurements Compared to Gaia

We compare the proper motions and positions of sources matched between the DECam and Gaia EDR3 catalogs. Our residual proper motion and position measurements are consistently smaller than our desired signal of 80 mas yr^{-1} (Figures 9 and 10), verifying the accuracy of the astrometric reference frame for our DECam measurements. We note that these matched stars were previously used to discover the polynomial transformation, so these do not provide a completely independent verification, but the fitting free parameters (30) are three orders of magnitude fewer than the sampled data points (∼8000 per CCD) so the correlations are not severe.

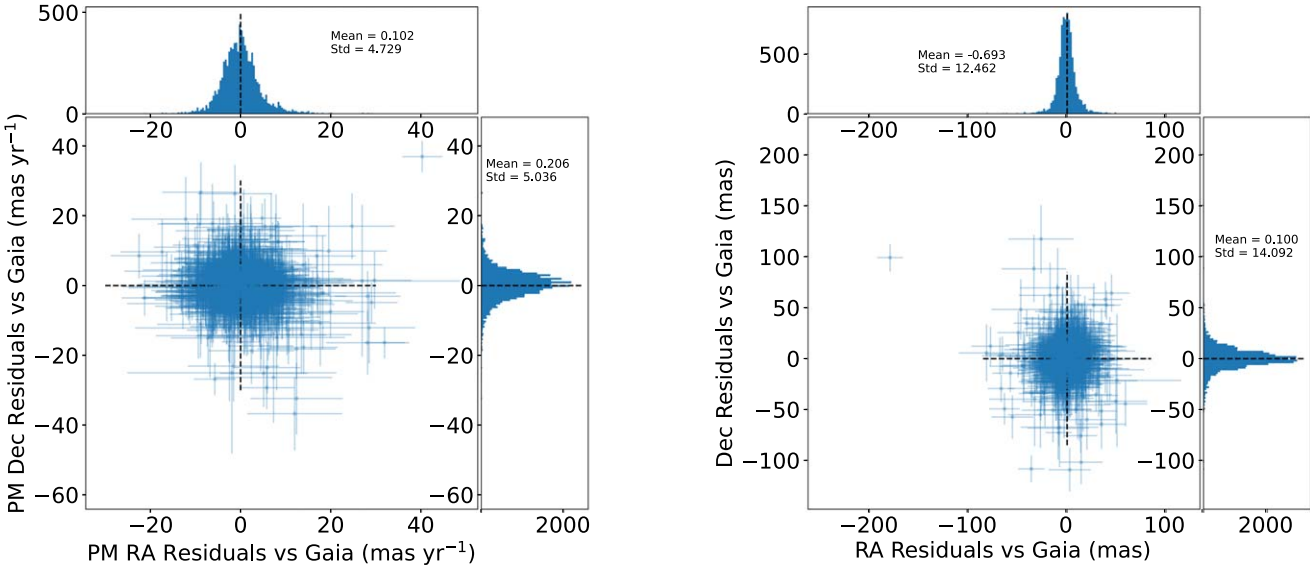

Figure 9. Residuals of DECam measurements vs. Gaia for cross-matched sources in R.A. and decl. in both proper-motion (left) and position (right) space. Our desired precision was 80 mas yr^{-1}, many times higher than the scatter in our distributions, which give an empirical estimate of our error.

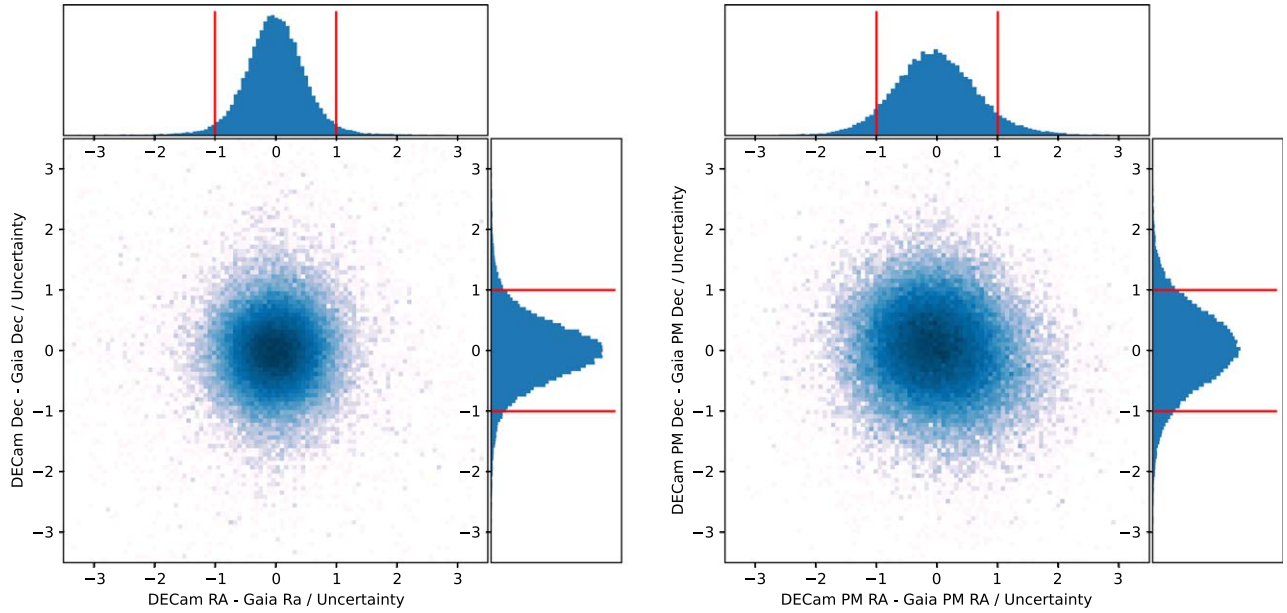

Figure 10. Position (left) and proper-motion (right) residuals of DECam vs. Gaia measurements for cross-matched sources in R.A. and decl. over uncertainty in each dimension. We expect 68% of sources to be smaller than 1σ. We find ∼92% of sources in position space and ∼85% of sources in proper-motion space lie within this region, suggesting that our errors may be overestimated.

ORCID iDs

Joshua V. Shields https://orcid.org/0000-0002-1560-5286
Wolfgang Kerzendorf https://orcid.org/0000-0002-0479-7235
Matthew W. Hosek, Jr. https://orcid.org/0000-0003-2874-1196
Ken J. Shen https://orcid.org/0000-0002-9632-6106
Armin Rest https://orcid.org/0000-0002-4410-5387
Tuan Do https://orcid.org/0000-0001-9554-6062
Jessica R. Lu https://orcid.org/0000-0001-9611-0009
Andrew G. Fullard https://orcid.org/0000-0001-7343-1678
Giovanni Strampelli https://orcid.org/0000-0002-1652-420X
Alfredo Zenteno https://orcid.org/0000-0001-6455-9135

References

Bertin, E., Mellier, Y., Radovich, M., et al. 2002, in ASP Conf. Proc. 281, Astronomical Data Analysis Software and Systems XI, 281, ed. D. A. Bohlender et al. (San Francisco, CA: ASP), 228
Bianco, F. B., Howell, D. A., Sullivan, M., et al. 2011, ApJ, 741, 20
Bloom, J. S., Kasen, D., Shen, K. J., et al. 2012, ApJ, 744, L17
Bradley, L., Deil, C., Patra, S., et al. 2022, astropy/regions: v0.5, Zenodo, doi:10.5281/zenodo.5826359
Brown, W. R. 2015, ARA&A, 53, 15
Capak 2019, Spitzer Enhanced Imaging Products (SEIP) Source List. doi:10.26131/IRSA3
Cartier, R., Sullivan, M., Firth, R. E., et al. 2017, MNRAS, 464, 4476
Colgate, S. A., & McKee, C. 1969, ApJ, 157, 623
Collaboration, G., Prusti, T., de Bruijne, J. H. J., et al. 2016, A&A, 595, A1
Collaboration, G., Brown, A. G. A., Vallenari, A., et al. 2018a, A&A, 616, A1
Collaboration, T. A., Price-Whelan, A. M., Sipőcz, B. M., et al. 2018, AJ, 156, 123

Dan, M., Rosswog, S., Guillochon, J., & Ramirez-Ruiz, E. 2011, ApJ, 737, 89
Diehl, T. 2012, PhPro, 37, 1332
Fausnaugh, M. M., Vallely, P. J., Kochanek, C. S., et al. 2021, ApJ, 908, 51
Fazio, G. G., Hora, J. L., Allen, L. E., et al. 2004, ApJS, 154, 10
Flaugher, B., Diehl, H. T., Honscheid, K., et al. 2015, AJ, 150, 150
Gaia Collaboration, Brown, A. G. A., Vallenari, A., et al. 2021, A&A, 649, A1
Generozov, A., & Perets, H. B. 2022, MNRAS, 513, 4257
Graham, M. L., Kumar, S., Hosseinzadeh, G., et al. 2017, MNRAS, 472, 3437
Green, D. A. 2019, JApA, 40, 36
Guillochon, J., Dan, M., Ramirez-Ruiz, E., & Rosswog, S. 2010, ApJ, 709, L64
Guo, H. L., Chen, B. Q., Yuan, H. B., et al. 2021, ApJ, 906, 47
Harris, C. R., Millman, K. J., van der Walt, S. J., et al. 2020, Natur, 585, 357
Hayden, B. T., Garnavich, P. M., Kessler, R., et al. 2010, ApJ, 712, 350
Hernandez, J. I. G., Ruiz-Lapuente, P., Tabernero, H. M., et al. 2012, Natur, 489, 533
Hernández, J. I. G., Ruiz-Lapuente, P., Filippenko, A. V., et al. 2009, ApJ, 691, 1
Hillebrandt, W., & Niemeyer, J. C. 2000, ARA&A, 38, 191
Hills, J. G. 1988, Natur, 331, 687
Holmbo, S., Stritzinger, M. D., Shappee, B. J., et al. 2019, A&A, 627, A174
Hunter, J. D. 2007, CSE, 9, 90
Iben, I., Jr., Nomoto, K., Tornambe, A., & Tutukov, A. V. 1987, ApJ, 317, 717
Iben, I., Jr., & Tutukov, A. V. 1984, ApJS, 54, 335
Ihara, Y., Ozaki, J., Doi, M., et al. 2007, PASJ, 59, 811
Kerzendorf, W. E., Childress, M., Scharwächter, J., Do, T., & Schmidt, B. P. 2014, ApJ, 782, 27
Kerzendorf, W. E., Long, K. S., Winkler, P. F., & Do, T. 2018, MNRAS, 479, 5696
Kerzendorf, W. E., Schmidt, B. P., Asplund, M., et al. 2009, ApJ, 701, 1665
Kerzendorf, W. E., Schmidt, B. P., Laird, J. B., Podsiadlowski, P., & Bessell, M. S. 2012, ApJ, 759, 7
Kerzendorf, W. E., Strampelli, G., Shen, K. J., et al. 2017, MNRAS, 479, 192
Kobayashi, C., Leung, S.-C., & Nomoto, K. 2020, ApJ, 895, 138
Leonard, D. C. 2007, ApJ, 670, 1275
Liu, Z.-W., Roepke, F. K., Zeng, Y., & Heger, A. 2021, A&A, 654, A103
Livio, M. 2000, in Type Ia Supernovae: Theory and Cosmology, The Progenitors of Type Ia Supernovae, ed. J. C. Niemeyer & J. W. Truran (Cambridge: Cambridge Univ. Press)
Lundqvist, P., Mattila, S., Sollerman, J., et al. 2013, MNRAS, 435, 329
Lundqvist, P., Nyholm, A., Taddia, F., et al. 2015, A&A, 577, A39
Maguire, K., Taubenberger, S., Sullivan, M., & Mazzali, P. A. 2016, MNRAS, 457, 3254
Maoz, D., Mannucci, F., & Nelemans, G. 2014, ARA&A, 52, 107
Marietta, E., Burrows, A., & Fryxell, B. 2000, ApJS, 128, 615
Marion, G. H., Brown, P. J., Vinkó, J., et al. 2016, ApJ, 820, 92
Mattila, S., Lundqvist, P., Sollerman, J., et al. 2005, A&A, 443, 649
Miller, A. A., Cao, Y., Piro, A. L., et al. 2018, ApJ, 852, 100
Nomoto, K. 1982, ApJ, 257, 780
Nomoto, K., Kobayashi, C., & Tominaga, N. 2013, ARA&A, 51, 457
Olling, R. P., Mushotzky, R., Shaya, E. J., et al. 2015, Natur, 521, 332
Pakmor, R., Kromer, M., Röpke, F. K., et al. 2010, Natur, 463, 61
Pakmor, R., Kromer, M., Taubenberger, S., & Springel, V. 2013, ApJ, 770, L8
Pakmor, R., Roepke, F. K., Weiss, A., & Hillebrandt, W. 2008, A&A, 489, 943
Pakmor, R., Callan, F. P., Collins, C. E., et al. 2022, arXiv:2203.14990
Pan, K.-C., Ricker, P. M., & Taam, R. E. 2012, ApJ, 750, 151
Pan, K.-C., Ricker, P. M., & Taam, R. E. 2013, ApJ, 773, 49
Pankey, T., Jr. 1962, PhD thesis, Howard Univ.
Perlmutter, S., Aldering, G., Goldhaber, G., et al. 1999, ApJ, 517, 565
Reback, J., & jbrockmendel, M. W. 2022, pandas-dev/pandas: Pandas 1.4.1 Zenodo, doi: 10.5281/zenodo.6053272, https://zenodo.org/record/6053272#.YrnstxPMLtW
Rest, A., Stubbs, C., Becker, A. C., et al. 2005, ApJ, 634, 1103
Rest, A., Scolnic, D., Foley, R. J., et al. 2013, ApJ, 795, 44
Riess, A. G., Filippenko, A. V., Challis, P., et al. 1998, AJ, 116, 1009
Ruiz-Lapuente, P. 2019, NewAR, 85, 101523
Ruiz-Lapuente, P., Damiani, F., Bedin, L., et al. 2018, ApJ, 862, 124
Ruiz-Lapuente, P., Comeron, F., Méndez, J., et al. 2004, Natur, 431, 1069
Ruiz-Lapuente, P., González Hernández, J. I., Mor, R., et al. 2019, ApJ, 870, 135
Sand, D. J., Hsiao, E. Y., Banerjee, D. P. K., et al. 2016, ApJ, 822, L16
Sand, D. J., Graham, M. L., Botyánszki, J., et al. 2018, ApJ, 863, 24
Schaefer, B. E., & Pagnotta, A. 2012, Natur, 481, 164
Schechter, P. L., Mateo, M., & Saha, A. 1993, PASP, 105, 1342
Schlafly, E. F., & Finkbeiner, D. P. 2011, ApJ, 737, 103
Shappee, B. J., Kochanek, C. S., & Stanek, K. Z. 2013a, ApJ, 765, 150
Shappee, B. J., Piro, A. L., Stanek, K. Z., et al. 2018, ApJ, 855, 6
Shappee, B. J., Stanek, K. Z., Pogge, R. W., & Garnavich, P. M. 2013b, ApJ, 762, L5
Shappee, B. J., Piro, A. L., Holoien, T. W. S., et al. 2016, ApJ, 826, 144
Shen, K. J., & Bildsten, L. 2014, ApJ, 785, 61
Shen, K. J., & Schwab, J. 2017, ApJ, 834, 180
Shen, K. J., Boubert, D., Gänsicke, B. T., et al. 2018, ApJ, 865, 15
The Astropy Collaboration, Robitaille, T. P., Tollerud, E. J., et al. 2013, A&A, 558, A33
Timmes, F. X., Woosley, S. E., & Weaver, T. A. 1995, ApJS, 98, 617
Tucker, M. A., Shappee, B. J., Vallely, P. J., et al. 2020, MNRAS, 493, 1044
Valdes, F., Gruendl, R. & DES Project 2014, The DECam Community Pipeline, in ASP Conf. Ser. 85, Astronomical Data Analysis Software and Systems XXIII, The DECam Community Pipeline, 485, ed. N. Manset & P. Forshay (San Francisco, CA: ASP), 379
Vallely, P. J., Fausnaugh, M., Jha, S. W., et al. 2019, MNRAS, 487, 2372
Virtanen, P., Gommers, R., Oliphant, T. E., et al. 2020, Nat. Methods, 17, 261
Webbink, R. F. 1984, ApJ, 277, 355
Werner, M. W., Roellig, T. L., Low, F. J., et al. 2004, ApJS, 154, 1
Whelan, J., & Iben, I., Jr. 1973, ApJ, 186, 1007
Williams, B. J., Borkowski, K. J., Ghavamian, P., et al. 2013, ApJ, 770, 129
Winkler, P. F., Gupta, G., & Long, K. S. 2002, ApJ, 585, 324
Winkler, P. F., Long, K. S., Hamilton, A. J. S., & Fesen, R. A. 2005, ApJ, 624, 189
Woods, T. E., Ghavamian, P., Badenes, C., & Gilfanov, M. 2017, NatAs, 1, 800
Zheng, W., Silverman, J. M., Filippenko, A. V., et al. 2013, ApJ, 778, L15